International Journal of Applied Engineering Research ISSN 0973-4562 Volume 10, Number 17 (2015) pp 37421-37427

Numerical and Experimental Study on the Heat Transfer Characteristics of the Micro-channel Heat Sinks with Longitudinal Fins Array

Parkpum Sriromreun
Department of Mechanical Engineering, Faculty of Engineering, Srinakharinwirot University,
63 Rangsit-Nakhornnayok Rd., Ongkharak, Nakhorn-Nayok, 26120, Thailand
E-mail address: sriromreun@yahoo.com

Paisarn Naphon*
Thermo-Fluid and Heat Transfer Enhancement Laboratory (TFHT),
Department of Mechanical Engineering, Faculty of Engineering, Srinakharinwirot University,
63 Rangsit-Nakhornnayok Rd., Ongkharak, Nakhorn-Nayok, 26120, Thailand
E-mail address: paisarnn@g.swu.ac.th
** Corresponding author,*

Abstract
The results of numerical and experimental study on the heat transfer characteristics in the micro-channel heat sinks with longitudinal fins under constant heat flux conditions are presented. The experiments are performed for verifying the predicted results from the mathematical model with the Reynolds number and heat flux in the ranges of 100-1200 and 1.50-5.50 kW/m^2, respectively. The micro-channel heat sink with two different channel heights and two different channel widths are tested. A numerical analysis of a three-dimensional transient model has been carried out to evaluate the thermal and fluid-dynamic performance. By solving the mathematical modeling, the velocity and temperature distributions of the heat sink section are presented. Reasonable agreement is obtained from the comparison with the measured data. These results are useful for the design to improve thermal performance of the heat sink, and also diminished the expense and time of the experiments.

Keywords; Numerical heat transfer; micro-channel heat sink; longitudinal fin

1. Introduction

For electronic devices, increasing demand for keeping/operating in the design temperature, higher performance and the level and reliability of the heat rejection largely require for these devices. At the conventional scale, heat sinks with various geometrical configurations have been used in various industries. However, the studies and applications of the micro-scale heat transfer devices for electronic cooling are still limited. Kayehpour et al. [1] and Chen [2] numerically studied the heat transfer and flow characteristics of gas flows in microchannels. Ambatirudi and Rahman [3] studied the heat transfer characteristics in microchannel heat sinks. Zhao and Lu [4] analytically and numerically studied effect of porosity on the thermal performance a micro channel heat sink. Honda and Wei [5] reviewed the papers concerning the two-phase boiling heat transfer of the dielectric in the micro-channel heat sink. Choi et al. [6] used the Langmuir slip condition to analyze the slip flow in microchannels. Hao and Tao [7] analyzed the two-phase heat transfer in the microchannels. Haddad and Abuzaid [8] observed the flow characteristics in the developing free-convection flow in a vertical open-ended microchannel with porous media. Zhang et al. [9] studied the single-phase heat transfer in the micro channel heat sink for electronic packages. Chein and Chuang [10] studied the heat transfer characteristics in the micro channel heat sink with and without thermoelectric using nanofluids as coolants. Kosar and Peles [11,12,13] studied the single-and two-phases heat transfer and flow phenomena of refrigerant in the micro pin fins heat sink. Tan and Ng [14] considered effect of EDL on heat transfer characteristic of 3-D developing flow in a microchannel. Zhen et al. [15] analyzed the 3-D and 2-D DSMC heat transfer of flow phenomena in the short microchannel. Hong and Asako [16] studied on the heat transfer characteristics of gaseous flows in a microchannel and a microtube. Chen [17] simulated the incompressible flow and heat transfer in microchannel. Hong et al. [18] analyzed the fluid and heat transfer characteristics in the microchannels. Lie [19] investigated the two-phase boiling heat transfer of FC-72 in a heated micro-pin-fin silicon chip. Lee and Son [20,21] observed the two-phase flow phenomena in a microchannel. Wang et al. [22,23] numerically studied the gas flow and heat transfer characteristics in a microchannel.

As mentioned above, the numerous works have been reported concerning the convective heat transfer in the heat sink with various geometrical configurations. However, only a few works reported on heat transfer characteristics and pressure drop in the micro-channel heat sink with longitudinal fins. In the present paper, the objective of this study is to study the convective heat transfer characteristics in the micro-channel heat sinks with longitudinal fins. The predicted results obtained from the model are verified with measured data.

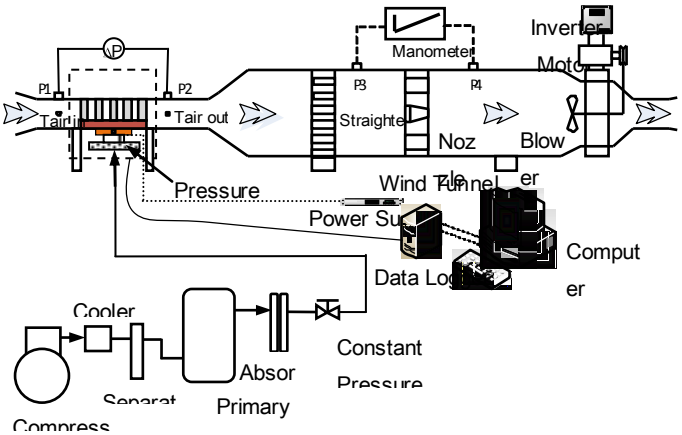

Fig. 1. Schematic diagram of experimental apparatus

2. Experimental Apparatus and Method

2.1 Experimental apparatus

A schematic diagram of the experimental apparatus is shown in Fig. 1. The test loop consists of a test section, chilled air loop and data acquisition system. The loop wind tunnel is rectangular air duct fabricated from acrylic (Solid Acrylic CO., LTD), having dimensions of 4*4 cm and the length of 150 cm. The duct is insulated with 5 mm thick Aeroflex standard sheet (Aeroflex Group CO., LTD). Air in the wind tunnel is suctioned by Axial fan into the channel and is passed through the test section, straightener, nozzle and then discharged to the atmosphere. The flow rate of air is measured by nozzle with the inclined tube manometer while the pressure drops across the test section are measured by the differential pressure transducer (Yokakawa) with an accuracy of 0.02% of full scale. There are four pressure taps on each wall upstream and downstream of the test section. The type T copper-constantan thermocouples with an accuracy of 0.1% of full scale are employed to measure air temperatures. The inlet and outlet temperatures of air are measured by two and four thermocouples with 1 mm diameter probes extending into the duct in which the air flows, respectively. All the thermocouples probes are precalibrated by dry-box temperature calibrator (Isotech) with 0.01^{o}C precision.

2.2 Test sections

The schematic diagram of the test section is shown in Fig. 2. The width and length of the heat sink are 28 and 40 mm, respectively. The micro-channel heat sinks with longitudinal fins are accomplished by the wire electrical discharge machine (WEDM). The micro-channel heat sink is placed inside the test section unit within a small gap to prevent any movement the heater position. Two channel width of 0.2, 0.3 mm and two channel height of 1.00, 1.50 mm the micro-channel heat sinks are tested. Air pressure is generated by air compressor system, the air regulator and toggle switch are used as pressure controller and switching the position of a cylinder, respectively. In the present study, air pressure is applied of 0.5 MPa to control stability pressure of cylinder. An AC power supply is the source of power for the plate type heaters. Rear face of the test section is insulated with a 10 mm thick heat-resistant Mica standard sheet, 5 mm thick Aeroflex standard sheet, and then 5 mm thick Acrylic standard sheet, respectively. Five type-T copper-constantan thermocouples with 1 mm diameter probes are used to measure the micro-channel heat sink wall temperature. The thermocouple is installed by mounting on the wall (drilled holes from the rear face) and fixed with special glue applied to the rear face of the walls. In order to minimize thermal contact resistance between the heat sink and the heater plate, a thin thermal interface material with high thermal conductivity is applied at their junction interface.

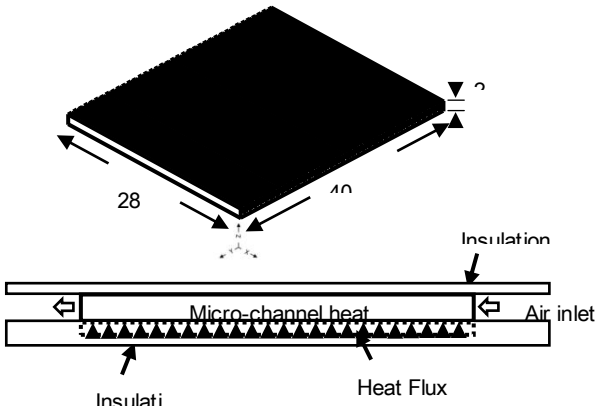

Fig. 2. Schematic diagram of the test channel and micro-channel heat sink

2.3 Experimental method

Experiments were conducted with various heat flux and flow rates of air entering the test section. In the experiments, air flow rate was increased in small increments while the supplied heat at the micro-channel heat sink was kept constant. The supplied heat into the micro-channel heat sink walls was adjusted to achieve the desired level by using electric heaters. The supplied power was calculated using the measured voltage and current supplied to the heaters. The supplied voltage and current to the heaters were measured by two digital clamp meters. The steady-state sensible heat gain by the air flow can be determined from an energy balance. The temperature at each position and pressure drop across the test section were recorded three times using a data acquisition system (Data Taker, DT85).

2.4. Data reduction and uncertainty analysis

The energy balance between the supplied heat by the heater plate and the absorbed heat by the coolant is ±10%. The average value of heat transfer rate is obtained from the supplied heat by heater plate and the absorbed heat by the coolant. The uncertainty and accuracy of the measurement are given in Table 1. The uncertainties of measurements data and the relevant parameters obtained from the data reduction process are calculated. The maximum uncertainties of the relevant parameters in the data calculation are based on Coleman and Steel method [24]. The maximum uncertainties of relevant parameters is 7.5% for the thermal resistance.

TABLE. 1. Accuracy and uncertainty of measurements

Instruments	Accuracy	Uncertainty
Voltage supplied, V	0.2%	$\pm$ 0.5
Current supplied, I	0.2%	$\pm$ 0.5
Thermocouple, T (°C)	0.1%	$\pm$ 0.1
Diff. Pressure Trans.	0.02%	$\pm$ 0.02

The data reduction of the measured data is summarized in the following procedures:
The average heat transfer rate, Q_{ave}, used in the calculation is determined from the heat removal my cooling air and the heat supplied to the micro-channel heat sink as follows:

$$Q_{ave} = \frac{Q_a + Q_{heater}}{2} \quad (1)$$

The average heat transfer coefficient of the micro-channel heat sink, h_m, can be calculated from the average heat transfer rate obtained from

$$Q_{ave} = h_m A_m \ \Delta T_{LMTD} \quad (2)$$

$$\Delta T_{LMTD} = \left[\frac{(T_{s,ave} - T_{a,ave,in}) - (T_{s,ave} - T_{a,ave,out})}{\ln\left(\frac{T_{s,ave} - T_{a,ave,in}}{T_{s,ave} - T_{a,ave,out}} \right)} \right] \quad (3)$$

where $T_{s,ave}$ is the average surface temperature, and A_m is the surface area of the micro-channel heat sink.
The average heat transfer coefficient is presented in term of average Nusselt number as follows:

$$Nu = \frac{h_m D_h}{\kappa} \quad (4)$$

$$D_h = \frac{4 \cdot A_{cross}}{P} \quad (5)$$

where k is the thermal conductivity of air, D_h is the hydraulic diameter of the channel before entering the test section, A_{cross} is the cross section area of the channel before entering the test section, and P is the wet perimeter of the channel.
The thermal resistance of the heat sink can be calculated from:

$$R_{tot} = \frac{T_{heat\sin k} - T_{a,inlet}}{Q_{ave}} \quad (6)$$

3. Mathematical modeling

3.1 Geometrical Model

A model of the micro-channel heat sink with longitudinal fins in the present study is shown in Fig. 3. The creation of the model geometry and its integration in a physical domain, grid generation and choice of a suitable numerical computing scheme are significant factors to obtain the optimized condition of success of the simulation process. In the present study, the commercial program ANSYS/FLUENT-14.0 is employed as the numerical solver to solve the model. The hardware on which is conducted the analysis a parallel computer system of distribution memory (cluster) and it is composed of 6 processors cores (12 Thread) with 64 GB memory RAM.

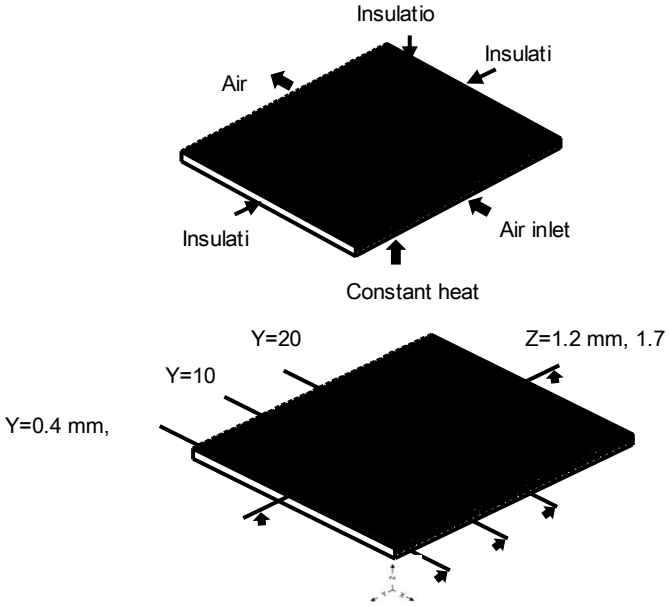

Fig. 3. Computational domain used in the present numerical study

3.2 Main governing equations

By considering the geometry and physical problem as shown in Fig. 3, the k-ε standard turbulence model [25] is employed to simulate the turbulent heat transfer characteristics. The computational domain is shown in Fig. 3 with the following assumptions:

- Air flow and heat transfer are in three dimensional.
- Single phase fluid flow is turbulent flow.
- Effects of gravitational force and radiation heat transfer are neglected.
- Properties of coolant and heat sink material are temperature independent.
- All the heat sink surfaces exposed to the surroundings are adiabatic

The main governing equations [25] can be written in the following form:

Continuity equation:

$$\frac{\partial \rho}{\partial t} + div \ \ \rho \mathbf{U} \ = 0 \quad (7)$$

Momentum equation:
x-momentum:

$$\rho \frac{Du}{Dt} = -\frac{\partial p}{\partial x} + div \ \ \mu \, grad \, u \ + S_{M_x} \quad (8)$$

y- momentum:

$$\rho\frac{Dv}{Dt}=-\frac{\partial p}{\partial y}+div\ \ \mu\, grad\, v\ \ +S_{M_y} \tag{9}$$

z- momentum:

$$\rho\frac{Dw}{Dt}=-\frac{\partial p}{\partial z}+div\ \ \mu\, grad\, w\ \ +S_{M_z} \tag{10}$$

Energy equation:

$$\rho\frac{Di}{Dt}=-p\,div\,\mathbf{U}+div\ \ \Gamma\, grad\, T\ \ +\Phi+S_i \tag{11}$$

Turbulent kinetic energy (k) equation:

$$\frac{\partial\ \rho k}{\partial t}+div\ \ \rho k\mathbf{U}\ =\ div\left[\left(\frac{\mu_t}{\sigma_k}grad\, k\right)\right]+ 2\mu_t E_{ij}\cdot E_{ij}-\rho\varepsilon \tag{12}$$

Turbulent kinetic energy dissipation (ε) equation:

$$\frac{\partial\ \rho\varepsilon}{\partial t}+div\ \ \rho\varepsilon\mathbf{U}\ =\ div\left(\frac{\mu_t}{\sigma_\varepsilon}grad\,\varepsilon\right)+ C_{1\varepsilon}\frac{\varepsilon}{k}2\mu_t E_{ij}\cdot E_{ij}-C_{2\varepsilon}\rho\frac{\varepsilon^2}{k} \tag{13}$$

The empirical constants for the turbulence model are arrived by comprehensive data fitting for a wide range of turbulent flow of Launder and Spalding [26]:

$$C_\mu=0.09,\ C_{\varepsilon 1}=1.47,\ C_{\varepsilon 2}=1.92,\ \sigma_k=1.0,\ \sigma_\varepsilon=1.3 \tag{14}$$

Boundary conditions:

In the present study, noslip and constant heat flux boundary conditions are applied on the test section as follows:

$$u=0, v=0, w=0, q=q_{wall} \tag{15}$$

where u,v,w are the velocities.

Initial conditions:

At the inlet boundary condition, the uniform profiles for all the properties are as follows:

$$u=u_{in}, v=0, w=0, T=T_{in}, k=k_{in}, \varepsilon=\varepsilon_{in} \tag{16}$$

The turbulent kinetic energy, k_{in}, and the turbulent kinetic energy dissipation, ε_{in}, at the inlet section are approximated from the turbulent intensity, *I*, and a turbulent characteristics length, *L*, as follows:

$$k_{in}=\frac{3}{2}\ u_{in}I^{\ 2},\ \ \varepsilon_{in}=C_\mu^{3/4}\frac{k^{3/2}}{L} \tag{17}$$

In the present study, the turbulence characteristics length, *L*, is set to be $0.07r_h$. The factor of 0.07 is based on the maximum value of the mixing length in the fully developed turbulent flow. The turbulent intensity level, *I*, is defined the ratio of the root-mean-square of the velocity fluctuation, u', to the mean flow velocity, u, as follows:

$$I=\frac{u'}{u}\times 100\% \tag{18}$$

3.3 Grid independent study

The 3D thermal and hydrodynamic models are used to solve for the heat transfer characteristics and fluid flow in the micro-channel heat sink with longitudinal fins walls. In the numerical results, the computational domain used in the present study is shown in Fig. 3. All of it, free wall surfaces are assumed adiabatic except bottom wall surface is heat dissipated. The transient model is based on the numerical solution of the governing equations of the mass, momentum and energy. Pressure–velocity coupling is achieved using the SIMPLE algorithm scheme [27]. The convergence criteria of 10^{-5} for the residual of the velocity component is assumed. In order to assess the accuracy of these computations, computational grids with 438,000, 833,000, 1,932,000 grids are used to test the grid independence of the solution as shown in Table 2. The grid independence tested indicated that the grid systems of 833,000 ensure a satisfactory solution.

TABLE. 2. Grid independent check

Grids	Outlet air temperature (°C)	%Errors
438,000	31.06	
833,000	31.39	1.06
1,932,000	31.28	0.35

3.4 Model verification

The steady-state sensible heat gain by the coolant flow can be determined from an energy balance. To validate the numerical model used in this study, the experimental works are carried to measure the results. Table 3 shows the comparison between the predicted outlet air temperature obtained from the model with the measured data. It can be seen that reasonable agreement is obtained from the comparison and gives the maximum error between the measured data and the predicted results about 11.54%.

TABLE. 3. Comparison between the predicted results and the measured data

Channel width (mm)	q (kW/m^2)	Air flow rate (m^3/s)	Outlet air temperature (^oC)		% Errors
			Measured results	Predicted results	
1.0*0.2	1.8	0.00033	37.39	33.45	11.12
		0.00042	36.52	32.67	11.13
		0.00050	35.95	32.10	11.32
1.0*0.3	1.8	0.00033	37.21	33.50	10.49
		0.00042	36.51	32.60	11.32
		0.00050	35.72	31.97	10.08
1.5*0.2	1.8	0.00033	37.34	33.13	11.95
		0.00042	35.77	32.64	9.15
		0.00050	35.12	31.36	11.31
1.5*0.3	1.8	0.00033	37.42	33.68	10.52
		0.00042	36.02	32.09	11.54
		0.00050	35.12	31.75	10.08

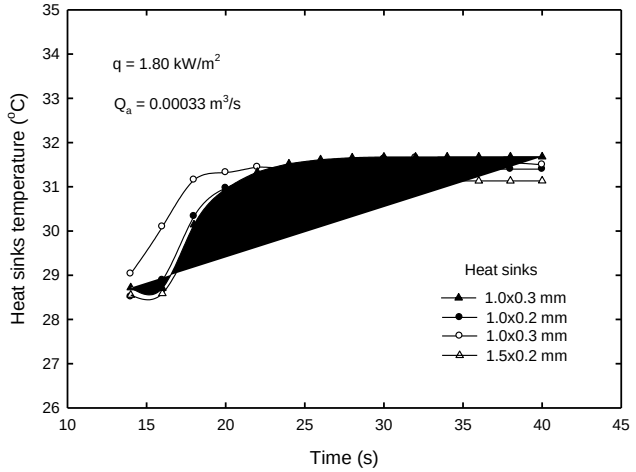

Fig. 4. Variation of micro channel heat sink temperature with time for different heat sinks

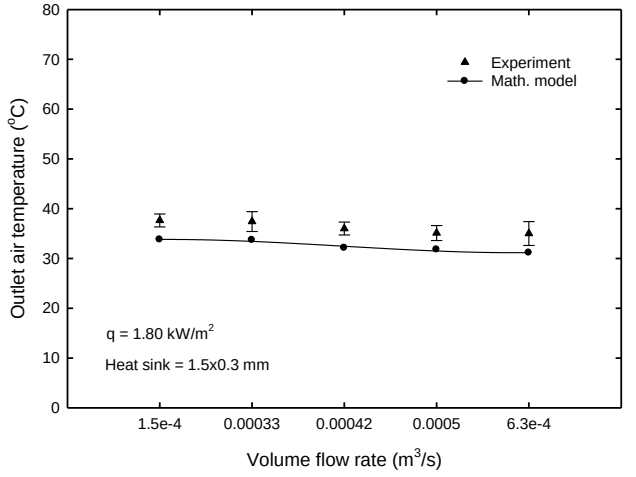

Fig. 5. Variation of outlet air temperature with coolant flow rate

4. Results and Discussion

As seen in Fig. 4, the higher surface heat transfer area, the lower channel width heat sink give average heat sink temperature slightly lower than that higher one. However, this parameter has slightly effect on average heat sink temperature. The reason for this is that the micro-channel widths are close in the present study. In addition, temperatures at higher channel height are lower than those from lower ones. Due to higher surface area and surface roughness, the heat transfer rate from the heat sink surface to the cooling air increases with increasing channel height. Therefore, the increase channel height results in lower heat sink temperatures as shown in Fig. 4. Figure 5 shows the variation of the outlet air temperature with air flow rate. Higher heat transfer rate as air flow rate increases. However, increase of heat transfer rate is less than that of air flow rate. Therefore, outlet air temperature tends to decrease as air flow rate increases. It can be seen that the results obtained from the model underpredicts the measured data with average error of 10.95%.

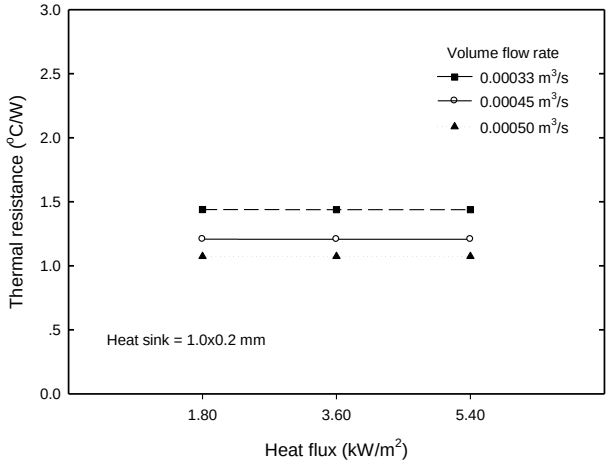

Fig. 6. Variation of thermal resistance of micro-channel heat sink with heat flux

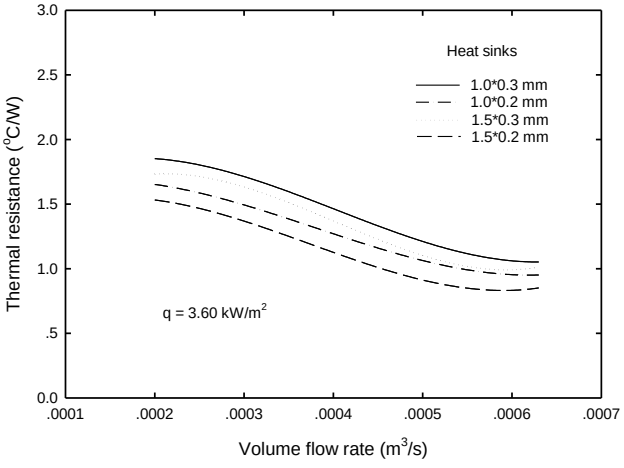

Fig. 7. Variation of thermal resistance of micro-channel heat sink with coolant flow rate for different heat sinks

Figure 6 shows the variation of thermal resistance with heat input for different air flow rate. It can be seen that heat flux is slightly significant effect on the total thermal resistance of the mini-channel heat sink. The total thermal resistance of the mini-channel heat sink is consisted of three terms thermal resistance; firstly, thermal resistance due to interface material; secondly, conduction thermal resistance and finally, convective thermal resistance. However, the total thermal resistance of the mini-channel heat sink is defined as the temperature difference between the heat source temperature and inlet air temperature divided with heat transfer rate as in Eq. (6). It can be clearly seen that the thermal resistance tends to decrease with increasing air flow rate. This is because the heat transfer rate from the heat sink to the coolant increases as air flow rate increases. Therefore, higher air flow rate results in lower thermal resistance as shown in Fig. 6.

Effect of channel configuration of the heat sink on the total thermal resistance is shown in Fig. 7. It can be seen that lower channel width (1.0*0.2 mm) gives the total thermal resistance lower than higher one (1.0*0.3 mm). Due to higher flow channel width, the coolant velocity tends to decrease and lower heat transfer rate which results in higher thermal resistance. For a given channel width, it can be seen that the heat sink with higher fin height (1.5*0.2 mm) gives thermal resistance lower than lower one (1.0*0.2 mm). This is because the heat transfer rate from the heat sink to the coolant depends on the heat transfer surface area. Therefore, the thermal resistance obtained from heat sink with fin height of 1.5* 0.2 mm is higher than from heat sink with fin height of 1.0*0.2 mm.

Figure 8 shows the temperature contour of the different micro-channel heat sinks. It can be seen from all heat sinks, the heat transfer is started from the inlet port and heat sink temperature tends to become higher along the heat sink. Therefore, the lower temperature different coolant and the heat sink, the heat transfer decreases along the heat sink.

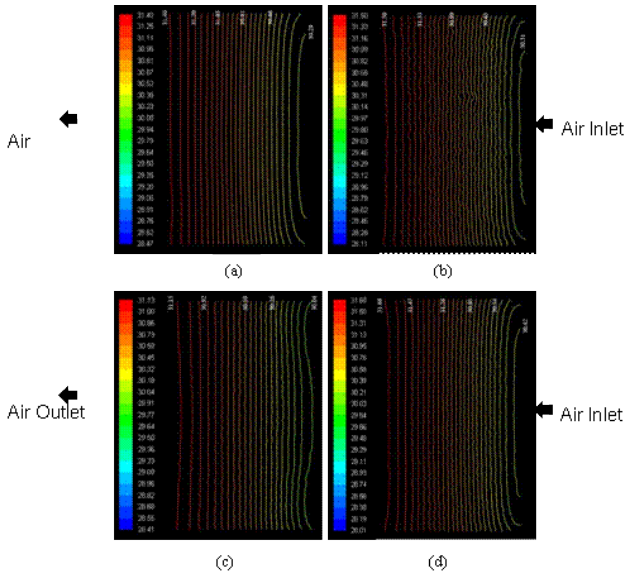

Fig. 8. Variation of temperature contour of the different micro-channel heat sinks

5. Conclusions

Due to higher performance, development of the miniaturized technologies, mini and micro-channel cooling systems have been widely used in the cooling system of the electronic devices. However, the heat transfer and fluid flow phenomena for the micro-channel are still limited. The heat transfer characteristics in the micro-channel heat sinks with longitudinal fins are investigated numerically and experimentally. It is found that the channel width and fin height have significant effect on the heat transfer and flow phenomena variations.

Nomenclature

A	area
$C_{1\varepsilon}$	turbulent model constant
$C_{2\varepsilon}$	turbulent model constant
C_{μ}	turbulent model constant
C_p	specific heat, kJ/(kg ^{o}C)
D_h	hydraulic diameter, m
h	heat transfer coefficient, W/(m^2 ^{o}C)
I	turbulent intensity
k	turbulent kinetic energy, m^2/s^2
L	turbulence characteristics length, m
Nu	Nusselt number
p	pressure, kPa
Pr	Prandtl number
P	wet perimeter, m
Q	heat transfer rate, kW
R_{tot}	thermal resistance, ^{o}C/W
Re	air Reynolds number
T	temperature, ^{o}C
$\mathbf{U}$	velocity vector
ε	dissipation kinetic energy, m^2/s^3
ρ	density, kg/m^3
μ	viscosity, kg/ms
Φ	viscosity energy dissipation function
σ_k	diffusion Prandtl number for k
σ_{ε}	diffusion Prandtl number for ε
κ	thermal conductivity, kW/(m ^{o}C)

Subscripts

a	air
ave	average
cr	cross section
in	*inlet*
out	*outlet*

Acknowledgements

The authors would like to express their appreciation to the Srinakharinwirot University (SWU) for providing financial support for this study.

References

[1] H.P. Kayehpour, M. Faghri, and Y. Asako, "Effects of compressibility and rarefaction on gaseous flows in microchannels," Numerical Heat Transfer, vol. 32, pp. 677-696, 1997.

[2] C.S. Chen, "Numerical analysis of gas flow in microchannels," Numerical Heat Transfer, vol. 33, pp. 749-762, 1998.

[3] K.H. Ambatirudi, and M.M. Rahman, "Analysis of conjugate heat transfer in microchannel heat sinks," Numerical Heat Transfer, vol. 37, pp. 711-731, 2000.

[4] C.Y. Zhao, and T.J. Lu, "Analysis of microchannel heat sink for electronics cooling," Int. J. Heat and Mass Transfer, vol. 45, pp. 4857-4869, 2002.

[5] J.J. Wei, and H. Honda, "Effects of fin geometry on boiling heat transfer from silicon chips with micro-pin-fins immersed in FC-72," Int. J. Heat and Mass Transfer, vol. 46, pp. 4059-4070, 2003.

[6] H.I. Choi, D. Lee, and J.S. Maeng, "Computation of slip flow in microchannels using Langmuir slip condition," Numerical Heat Transfer, vol. 44, pp. 59-71, 2003.

[7] Y.L. Hao, and Y.X. Tao, "A numerical model for phase-change suspension flow in microchannels," Numerical Heat Transfer, vol. 46, pp. 55-77, 2004.

[8] O.M. Haddad, and M.M. Abuzaid, "Developing free-convection gas flow in a vertical open-ended microchannel filled with porous media," Numerical Heat Transfer, vol. 48, pp. 693-710, 2005.

[9] H.Y. Zhang, "Single- phase liquid cooled micro channel heat sink for electronic packages," Applied Thermal Engineering, vol. 25, pp. 1472-1487, 2005.

[10] R. Chein, and Y. Chen, "Performance of thermoelectric cooler integrated with microchannel heat sinks," Int. J. Refrigeration, vol. 28, pp. 828-839, 2005.

[11] Y. Peles, "Forced convective heat transfer across a pin fin micro heat sink," Int. J. Heat and Mass Transfer, vol. 48. pp. 3615-3627, 2005.

[12] A. Kosar, and Y. Peles, "Convective flow of refrigerant (R123) across a bank of micro pin fins," Int. J. Heat and Mass Transfer, vol. 49, pp. 3142-3155, 2006.

[13] A. Kosar, and Y. Peles, "Boiling heat transfer in a hydrofoil-based micro pin fin heat sink," Int. J. Heat and Mass Transfer, vol. 50, pp. 1018-1034, 2007.

[14] S.T. Tan, and E.Y.K. Ng, "Numerical analysis of EDL effect on heat transfer characteristic of 3-D developing flow in a microchannel," Numerical Heat Transfer, vol. 49, pp. 991-1007, 2006.

[15] C.E. Zhen, Z.C. Hong, Y.J. Lin, and N.T. Hong, "Comparison of 3-D and 2-D DSMC heat transfer calculations of flow-speed short microchannel flows," Numerical Heat Transfer, vol. 52, pp. 239-250, 2007.

[16] C. Hong, and Y. Asako, "Heat transfer characteristics of gaseous flows in a microchannel and a microtube with constant wall temperature," Numerical Heat Transfer, vol. 52, pp. 219-238, 2007.

[17] C.S. Chen, "Reduced Navier-Strokes simulation of incompressible microchannel flows," Numerical Heat Transfer, vol. 53, pp. 71-87, 2007.

[18] Z.C. Hong, C.E. Zhen, and C.Y. Yang, "Fluid dynamics and heat transfer analysis of three dimensional microchannel flows with microstructures," Numerical Heat Transfer, vol. 54, pp. 293-314, 2007.

[19] Y.M. Lie, "Saturated flow boiling heat transfer and associated bubble characteristics of FC-72 on a heated micro-pin-fined silicon chip," Int. J. Heat and Mass Transfer, vol. 50, pp. 3862-3876, 2007.

[20] W. Lee, and G. Son, "Bubble dynamics and heat transfer during nucleate boiling in a microchannel," Numerical Heat Transfer, vol. 53, pp. 1074-1090, 2008.

[21] W. Lee, Y. Suh, and G. Son, "Bubble dynamics, flow, and heat transfer during flow boiling in parallel microchannels," Numerical Heat Transfer, vol. 54, pp. 390-405, 2008.

[22] Q.W. Wang, C.L. Zhao, M. Zeng, and Y.N. Wu, "Numerical investigation of rarefied diatomic gas flow and heat transfer in a microchannel using DSMC with uniform heat flux boundary condition-Part I: Numerical method and validation," Numerical Heat Transfer, vol. 53, pp. 160-173, 2008.

[23] Q.W. Wang, C.L. Zhao, M. Zeng, and Y.N. Wu, "Numerical investigation of rarefied diatomic gas flow and heat transfer in a microchannel using DSMC with uniform heat flux boundary condition-Part II: Applications," Numerical Heat Transfer, pp. 53, pp. 174-187, 2008.

[24] Coleman, H.W., and Steele, W.G., 1989, "Experimental and Uncertainty Analysis for Engineers," John Wiley&Sons, New York.

[25] H.K. Versteeg, and W. Malalasekera, "Computational fluid dynamics," Longman Group, 1995.

[26] B.E. Launder and D.B. Spalding, "Mathematical models of turbulence," Academic Press., 1973.

[27] J.P. Van Doormal and G.D. Raithby, "Enhancement of the SIMPLEC method for predicting incompressible fluid flows," Numerical Heat Transfer, vol. 7, pp. 147-163, 1984.